ADVANCED MODELLING OF FATIGUE CRACK PROPAGATION IN AIRCRAFT STRUCTURES FOR LONGER ASSURED LIFE AND INSPECTION INTERVALS

STAGE 2 IRAD STATEMENT OF WORK TO BE PERFOMED BY FATIGUE TECHNOLOGY ASSOCIATES

K. F. Walker
Senior Principal Engineer
QinetiQ Pty Ltd
210 Kingsway
South Melbourne VIC 3205
Australia

Total Cost:

10 November 2022

CONTENTS

1. Project Background

Fatigue-crack growth in metallic materials has been studied for the past 70 years. The Comet airplane failures in the mid-1950's was instrumental in starting research programs world-wide by many aircraft companies and universities to understand the controlling factors. The development of the principles of Fracture Mechanics, especially the crack-tip stress-intensity factor (K), has provided aircraft designers with a methodology to predict fatigue lives and fatigue-crack growth lives of complex metallic components. In the mid-1960's, the phenomenon on flat-to slant crack growth, as shown in Figure 1, was studied by many in the aircraft industry [1]. At low stress-intensity factors, a crack surface is very flat, and the behavior is referred to as the tensile crack-growth mode. In addition, the stress state in the crack front is under plane-strain conditions or what is called high constraint. As the crack grows with higher stress-intensity factors, a 45-degree shear lip starts to develop at the intersection of the crack front and the free surfaces. At a certain point, with further crack extension, a complete shear failure occurs through the thickness of the sheet or plate. This behaviour is the shear mode, which is under low constraint or plane-stress conditions.

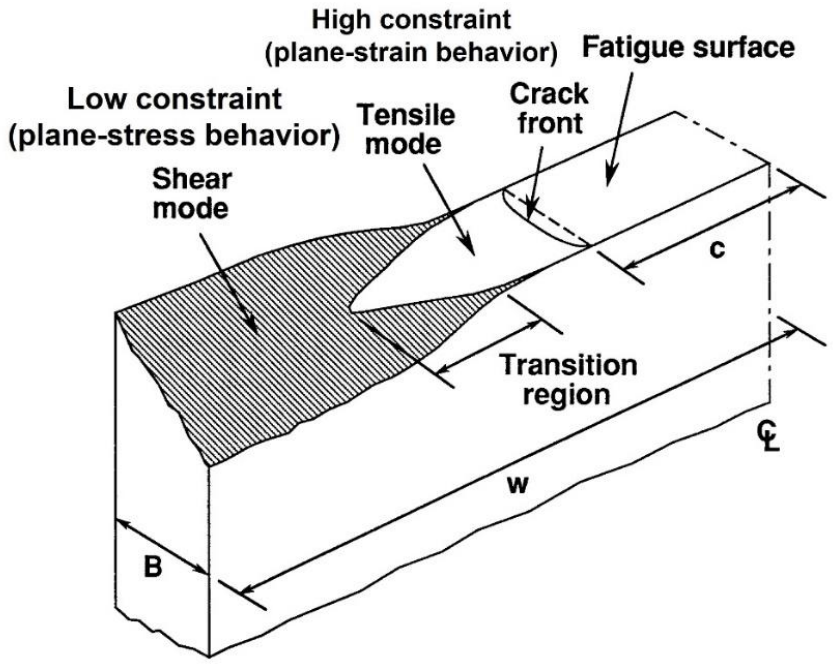

Figure 1 – Schematic of flat-to-slant fatigue-crack growth in metallic materials.

In 1966, Schijve [2] found that the transition from flat-to-slant crack-growth behaviour occurred at a "constant" rate, independent of R. Others at the ASTM Symposium on Crack Propagation [1] had proposed that ΔK or K_{max} controlled the transitional behavior. However, Newman [3] in a discussion on the subject had provided additional test data from the NASA Langley Research Centre to support Schijve's conclusion that crack-growth rate was the controlling parameter.

In studying fatigue-crack growth in 2024-T3 aluminium alloy, Elber [4] discovered the crack-closure phenomenon, whereby the crack surfaces are partially closed under tensile loading. Cracks only grow when the crack tip is fully open. He proposed that the effective stress-intensity factor, ΔK_{eff}, controlled the fatigue-crack-growth rates as

$$\Delta K_{eff} = (S_{max} - S_o) \sqrt{(\pi\, c)}\, F \qquad (1)$$

The plasticity-induced crack closure (PICC) concept has revolutionized the analyses of crack growth under constant- and variable-amplitude loading. Elber found that the measured crack-opening values at various stress ratios ($R = S_{min}/S_{max}$) was able to collapse the crack-growth-rates onto a nearly unique relation between ΔK_{eff} and rate. Since Schijve showed that flat-to-slant crack growth occurred at a constant rate, then Elber's relation would indicate the ΔK_{eff} controls the flat-to-slant (plane-strain to plane-stress) crack growth. In 1992, Newman developed a relationship to predict the location on the flat-to-slant crack-growth region. However, the range of the constraint-loss regime had to be determined by trial-and-error using spectrum loading tests.

2. Stage I Project Description

The materials used in the proposed project, 2024-T3 and 7075-T6, are NASA Langley Research Centre stock materials procured in the 1950's, since these two materials are widely used in aerospace applications. These materials have been extensively studied for tensile properties, fatigue, fatigue-crack growth, and fracture; and the results are presented in many NACA and NASA reports.

The project has three main areas of research: (1) constraint-loss behaviour, (2) fracture behaviour, and (3) single-spike overload behaviour. In addition, the FASTRAN [5, 6] life-prediction code will be used to correlate and to calculate the crack-growth behaviour during constraint loss and the various test results on the single-spike overloads. The main objectives are to see if the constraint-loss region can be experimentally measured and whether constraint-loss behaviour is the primary reason for crack-growth delays after single-spike overloads. These results are very important. If the current crack-growth models cannot predict the delay cycles from a simple spike overload, then are the models accurate under more complex aircraft spectrum loading.

Phase I was to conduct some preliminary tests to measure the constraint-loss regime during constant-amplitude fatigue-crack growth tests, and to start development of a method to determine the constraint-loss regime from fatigue-crack-growth-rate data. Conduct single-spike overload tests to demonstrate the importance of the proper location of the constraint-loss regime. Provide a roadmap for future testing to demonstrate the importance of the constraint-loss regime for predicting crack-growth life under aircraft spectrum loading.

3. Aluminium 7075-T6 Alloy

Two pieces of 7075-T6 thin-sheet material (B = 2.3 mm) had 18 middle-crack tension, M(T), machined with a total width (2w) of 96.5 mm. Total length between friction grips was about 200 mm. Anti-buckling guide plates were always used for fracture testing, but guides were not used for fatigue-crack-growth testing. Two holes were drilled and tap for mounting crack-mouth-opening-displacement, CMOD, gauges. The CMOD gauges were used for monitoring crack growth and recording the load-CMOD record for determining the crack-opening load using the FTA Crack-Monitoring System [7]. To help minimize the electronic and mechanical noise from the CMOD gauges, tests were conducted at low test frequencies (0.5 to 2 Hz).

3.1 Constant-Amplitude Loading

Herein, the results of some preliminary fatigue-crack-growth tests on M(T) specimens are made and compared with previous test data from NASA Langley Research Centre (LaRC) on the same material [8-11]. Figure 2 shows ΔK against crack-growth rate (dc/dN) for R = 0 and 0.5 loading. The two horizontal lines show the start and end of the constraint-loss regime that was determined many years ago by trial-and-error procedures. The new test data are shown as Test B1 and B5, which compared well over more than 2-orders of magnitude in rates under low-R conditions. The open circular symbols are NASA tests at R = 0.5 [11]. The light grey symbols are ΔK_{eff} data determined from the FTA Crack-Monitoring System using the zero-percent compliance offset values from the two low-R tests. The measured ΔK_{eff}-rate data agreed well with the ΔK_{eff} curve (blue lines with circular yellow symbols) established many years ago.

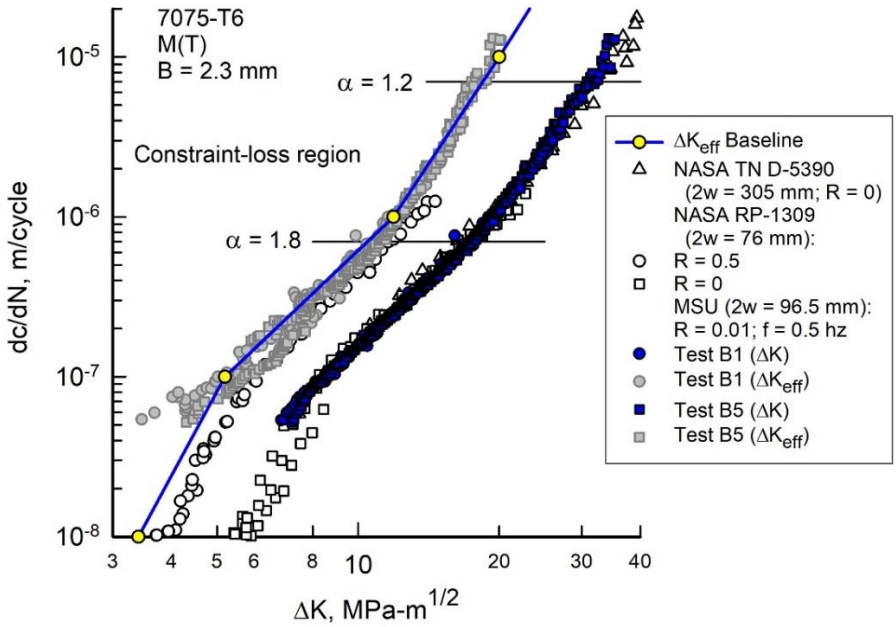

Figure 2 – Elastic stress-intensity factor range against rate for 7075-T6 at low and high R.

3.2 Fracture

Because the end of the constraint-loss regime for the 7075-T6 alloy was very close to fracture, tests were conducted on a few specimens over a wide range in crack-length-to-width (c_i/w) ratio to allow accurate prediction of failure. Anti-buckling guide plates were used in the fracture tests to help prevent buckling. The elastic stress-intensity factor, K_{Ie}, at fracture is plotted against c_i/w ratio in Figure 3, as open square symbols. The open circular symbols are test data from Hudson and Scardina [8, 9] on larger width specimens. The larger width specimens failed at large values of K_{Ie} than the smaller width specimens.

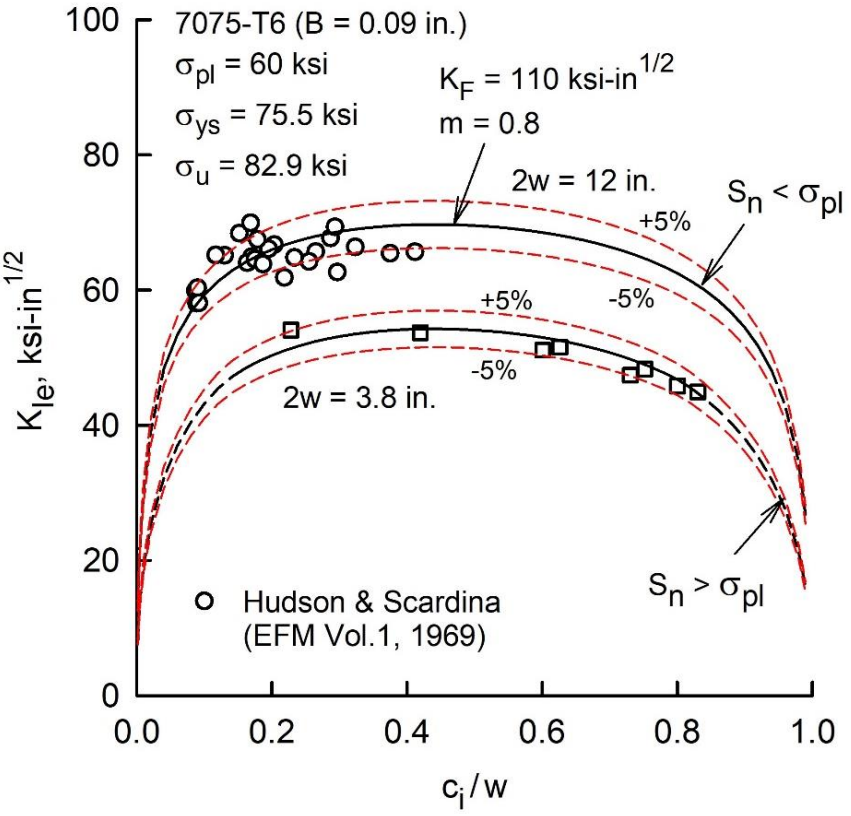

Figure 3 – Elastic stress-intensity factor at failure on 7075-T6 thin-sheet alloy.

The Two-Parameter Fracture Criterion (TPFC) [12] was used to analyse the fracture data on the M(T) specimens from NASA and those recently tested. A trial-and-error method was used to determine K_F and m. The solid curves in Figure 3 are predicted K_{Ie} values against c_i/w for the two widths. Fracture on the smaller width specimens fell within 5% (upper and lower dashed curves) of the predicted behaviour. The tests on the wider specimens tested at NASA showed larger scatter, but 75% of the test failures fell within +/- 5%.

3.3 Constraint-Loss Behaviour

The tests at low R were designed to propagate the crack across the constraint-loss regime. Crack-opening loads were measured from the FTA System [7]. Again, the zero-percent compliance offset values was determined from the 1 and 2% offset values as OP0 = 2 OP1 – OP2. (OPn is the compliance offset value at n-percent.) Figure 4 shows P_o/P_{max} plotted against c/w ratio. The horizontal dashed lines show the crack-opening-load ratio for plane-strain (α = 3) and plane-stress (α = 1) behavior. Tests B1 and B5 were tested at S_{max} = 50 MPa and R = 0.1 at 0.5 hz, which showed a rise in the crack-opening ratio for c/w > 0.55. Test B7 was tested at a higher applied stress level (S_{max} = 75 MPa; R = 0.01) and the test showed a rise in crack-opening ratios for c/w > 0.3. Measurements of P_o/P_{max} from the experiments showed large scatter but showed the correct trend. Solid curves were calculated crack-opening-load ratios from FASTRAN using the current constraint-loss regime (see Fig. 2).

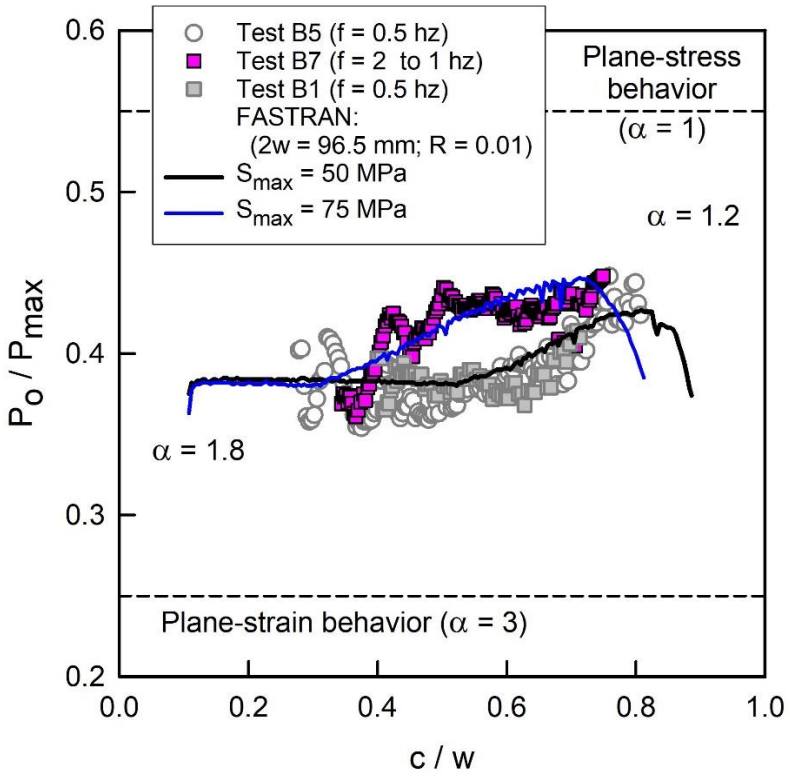

Figure 4 – Crack-opening-load ratio during constraint-loss regime on 7075-T6.

3.4 Single-Spike Overload/Underload Testing

Figure 5 shows the loading sequence to be applied during the repeated single-spike overload/underload testing. A crack will be grown from the crack-starter notch under constant-amplitude (CA) loading at a given maximum load

level and R for N_{CA} cycles. A single-spike overload at OL value will be statically applied, and then an under load at UL value will be applied. CA loading continued until steady-state behaviour was achieved. Then another OL and UL will be applied, and the crack grown under CA loading to a specified crack length. The specimen will then be pulled to failure to determine the fracture toughness.

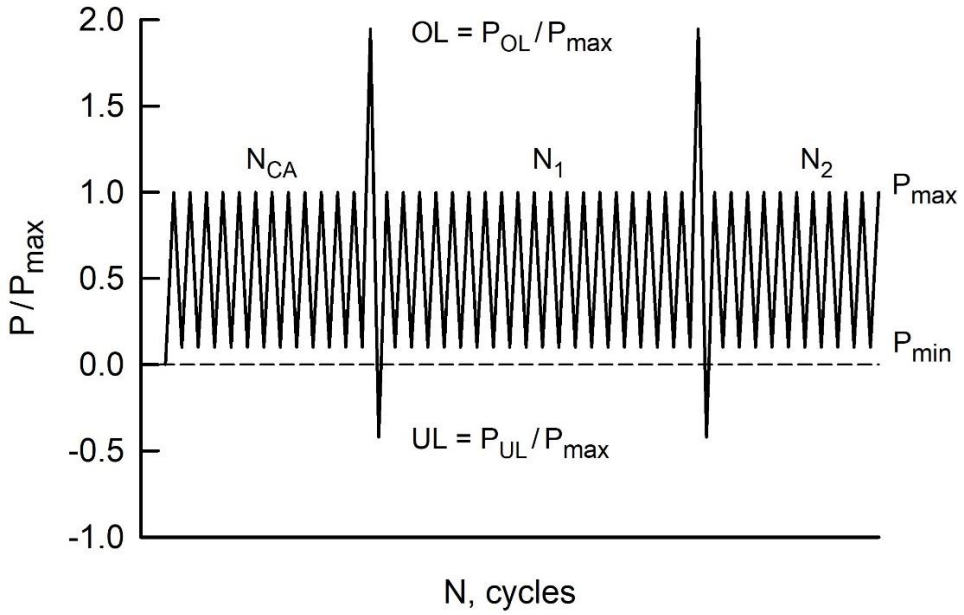

Figure 5 – Single-spike overload and underload test sequence.

The results of a repeated single-spike overload/underload test (solid circular symbols) are shown in Figure 6 on a 7075-T6 M(T) specimen. Test B8 was subjected to S_{max} = 75 MPa at R = 0.01 and frequency (f) of 2 hz. Crack was initiated at the crack-starter notch (c_n = 5 mm) and grown to c = 10 mm. Here, a factor of 2 overload (150 MPa) was statically applied and then unloaded to zero (UL = 0). CA loading resumed and the crack was grown to 15 mm, where another factor of 2 overload was applied.

FASTRAN [6] was used to predict crack growth using the ΔK_{eff}-rate curve (see Fig. 2) and constraint-loss regime that had previously been determined for the thin-sheet alloy. The dashed curve is under CA loading while the solid (blue) curve is under the repeated spike overload/underload test. The model over predicted the delay from the first overload but was reasonable for the second overload. These results suggest that the start of the constraint-loss regime (CLR) needs to be moved to a slightly higher rate, so that less delay will occur. The dash-dot curve shows the results for constant constraint (α = 1.8), which predicted very little crack-growth delay after both overloads.

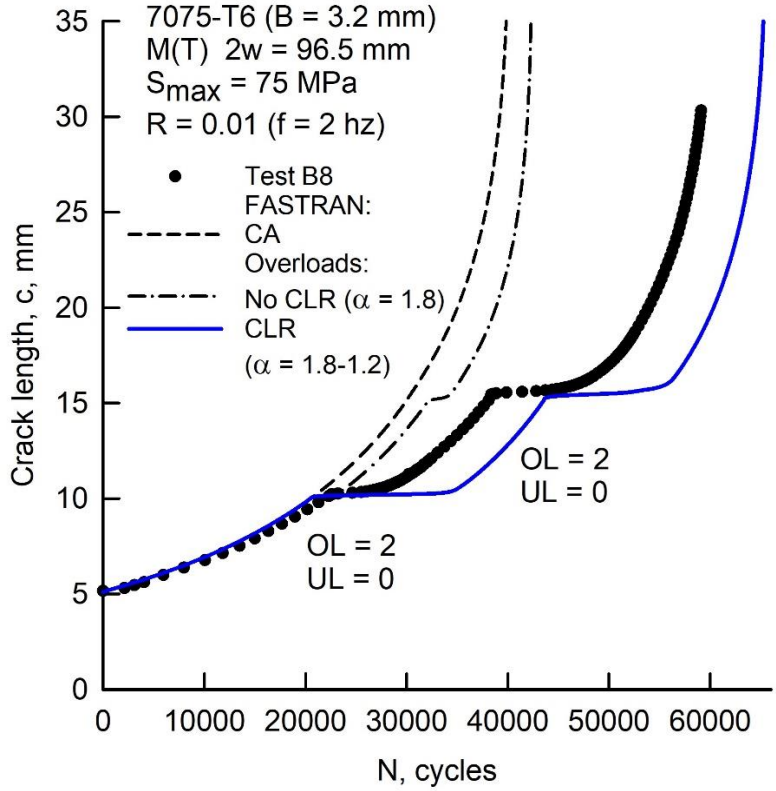

Figure 6 – Single-spike overload and underload sequence on a 7075-T6 specimen.

4. Aluminium 2024-T3 Alloy

Two pieces of 2024-T3 thin-sheet material (B = 2.3 mm) had 18 middle-crack tension, M(T), machined with a total width (2w) of 96.5 mm. Total length between friction grips was about 200 mm. Anti-buckling guide plates were always used for fracture testing, but guides were not used for fatigue-crack-growth testing. Two holes were drilled and tap for mounting crack-mouth-opening-displacement, CMOD, gauges. The CMOD gauges were used for monitoring crack growth and recording the load-CMOD record for determining the crack-opening load using the FTA Crack-Monitoring System [7].

4.1 Constant-Amplitude Loading

Some preliminary results on fatigue-crack-growth tests conducted on the 2024-T3 M(T) specimens. These data are compared with previous test data from NASA LaRC on the same material [9, 10, 13]. Figures 7 and 8 show ΔK against crack-growth rate for R = 0.7 and 0 loading, respectively. Two horizontal lines on each figure show the start and end of the constraint-loss regime that was determined by trial-and-error procedures. One test at R = 0.7 (A2) and two tests at R = 0 (A1, A3) produced ΔK-rate data slightly faster than the NASA LaRC data. NASA data [9] in the mid-region (10^{-8} to 10^{-6} m/cycle) was tested with the use of pink alcohol to enhance visual crack length measurements.

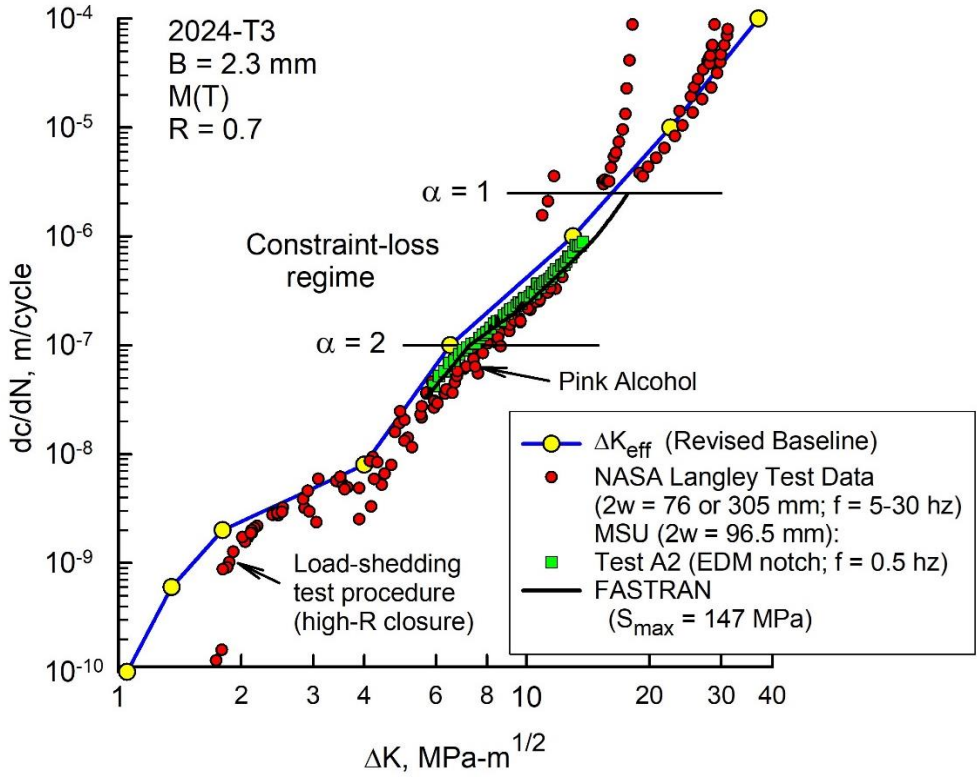

Figure 7 – Elastic stress-intensity factor range against rate for 2024-T3 at high R.

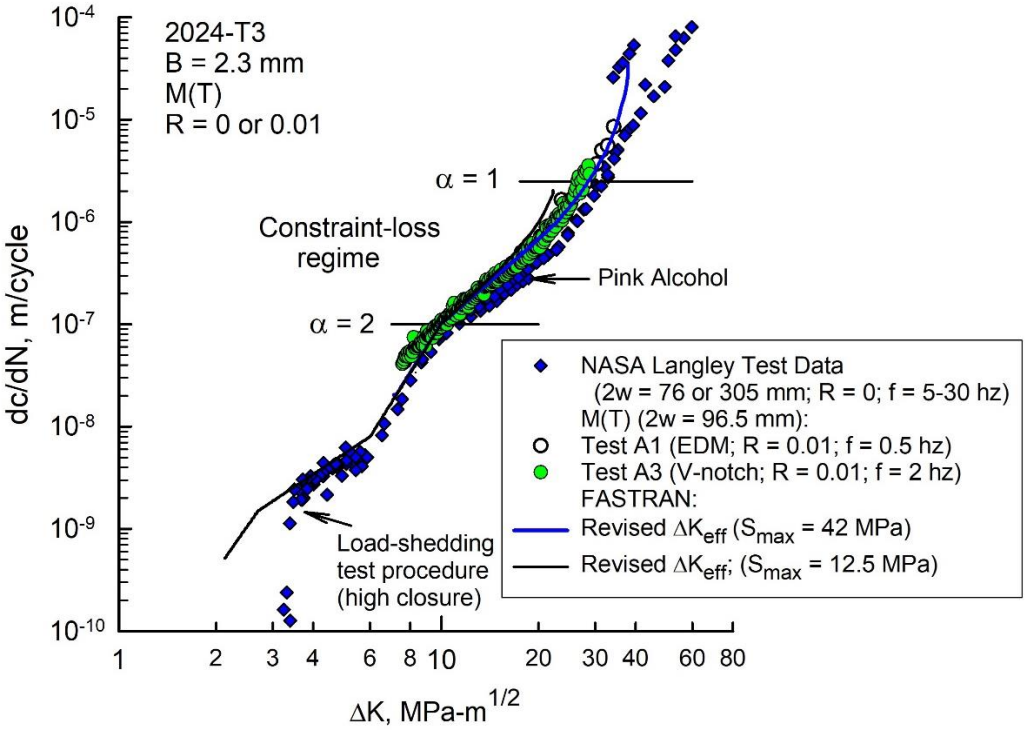

Figure 8 – Elastic stress-intensity factor range against rate for 2024-T3 at low R.

(In the early 1970's, the use of "pink alcohol" at NASA LaRC was prohibited.) NASA test data in the fracture region [10] and in the low-rate (threshold) region [13] did not use pink alcohol. However, test data in the threshold region used the ASTM E-647 [14] load-shedding method, which has been shown to cause a load-history effect that produces elevated thresholds and slower rates that steady-state behaviour.

The original ΔK_{eff}-rate baseline curve was fit to the NASA LaRC data, some of which had used pink alcohol to enhance crack length measurements, so some slight modifications were made to the ΔK_{eff}-rate curve in the mid-rate region. The solid curves on Figures 7 and 8 were calculated ΔK-rate behaviour using the FASTRAN code with the revised ΔK_{eff} curve.

4.2 Fracture

For the thin-sheet 2024-T3 alloy, the end of the constraint-loss regime is well below the crack-growth rate at fracture, see Figure 8. However, fracture tests are needed to accurately predict failure, so that fatigue-crack-growth tests can be used to generate data at very high rates. Anti-buckling guide plates were used in the fracture tests to help prevent buckling. The elastic stress-intensity factor, K_{Ie}, at fracture is plotted against c_i/w ratio in Figure 9. The circular symbols are test data from Newman [15] on larger width specimens. The larger width specimens failed at large values of K_{Ie} than the smaller width specimens.

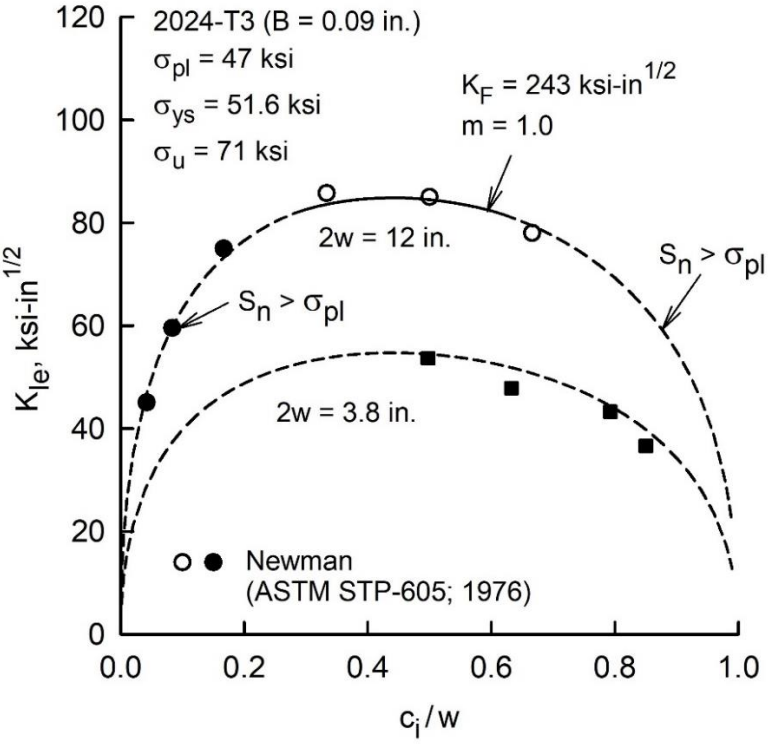

Figure 9 – Elastic stress-intensity factor at failure on 2024-T3 thin-sheet alloy.

Again, the Two-Parameter Fracture Criterion (TPFC) [12] was used to analyse the fracture data on the M(T) specimens from NASA and those recently tested. A trial-and-error method was used to determine K_F and m. The solid and dashed curves in Figure 9 are predicted K_{Ie} values against c_i/w for the two widths. The TPFC worked extremely well on the more ductile 2024-T3 alloy.

4.3 Constraint-Loss Behaviour

Because the measured crack-opening load ratios, even at low test frequencies, show a large amount of scatter, an alternate method to determine the constraint-loss regime is proposed. It has been observed that the spread in the ΔK-rate with the R value is a function of the constraint factor. For example, Figure 10 shows the ΔK_{eff}-rate relation (blue curve) and the ΔK-rate data at low R. For a given rate, the spread between the two curves can be used to evaluate the appropriate constraint factor, α. A larger spread means a lower constraint factor.

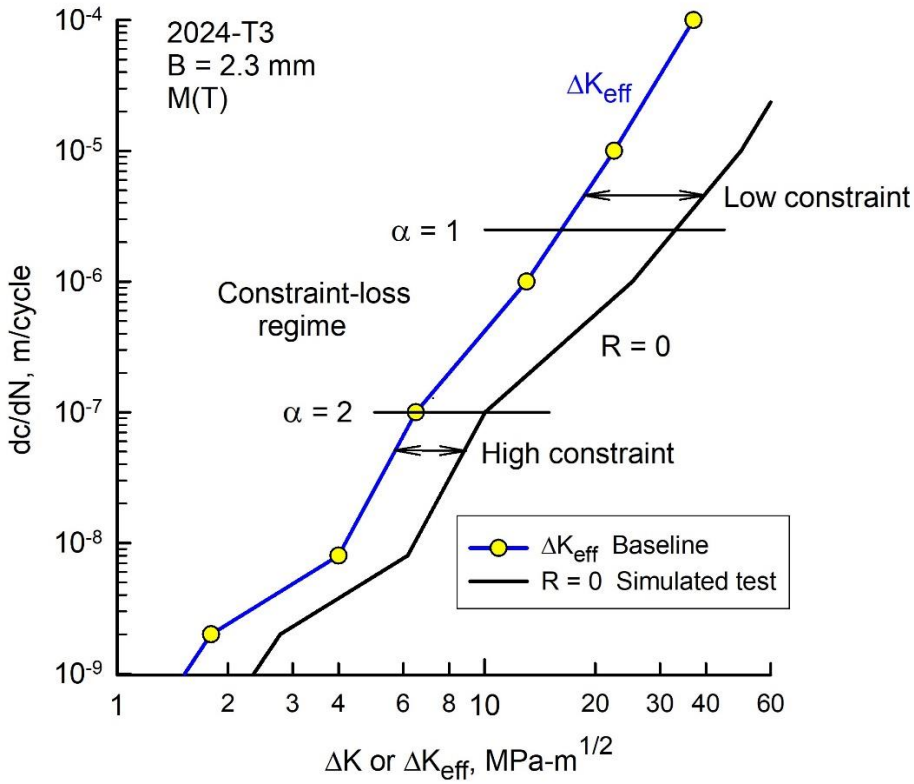

Figure 10 – Schematic of method to determine constraint-loss regime from fatigue-crack-growth-rate data in metallic materials.

4.4 Single-Spike Overload/Underload Testing

The results of a repeated single-spike overload/underload test (solid circular symbols) are shown in Figure 11 on a 2024-T3 M(T) specimen. Test A4 was subjected to S_{max} = 55 MPa at R = 0.01 and frequency (f) of 2 hz. Crack was initiated at the crack-starter notch (c_n = 9 mm) and grown to c = 14 mm. Here, a factor of 2 overload (110 MPa) was statically applied and then unloaded to zero (UL = 0). CA loading resumed and the crack was grown to 19 mm, where another factor of 2 overload was applied.

FASTRAN [6] was used to predict crack growth using the ΔK_{eff}-rate curve (see Fig. 7) and constraint-loss regime that had previously been determined for the thin-sheet alloy. The dashed curve is under CA loading while the solid (blue) curve is under the repeated spike overload/underload test. The model predicted the delay from the first and second overloads very well. These results indicate that the constraint-loss regime (CLR) location is good. The solid (black) curve shows the results for constant constraint (α = 2), which predicted very little crack-growth delay after both overloads.

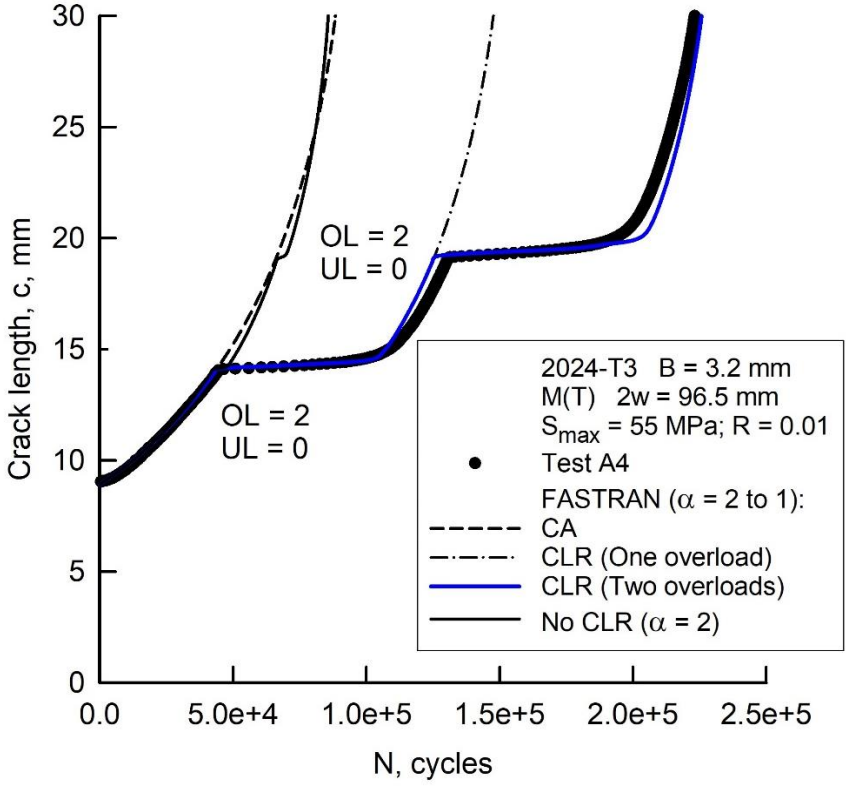

Figure 11 – Single-spike overload and underload sequence on a 2024-T3 specimen.

5. Stage 2 Testing

A large number of M(T) specimens (18 for 7075-T6; 18 for 2024-T3) are available for testing in Stage 2. In Stage I, four 2024-T3 and seven 7075-T6 specimens were tested under constant-amplitude loading; and another specimen of each material was tested under single-spike overloads. These specimens were used to validate the ΔK-rate data for several stress (S_{min}/S_{max}) ratios and to study the fracture toughness behaviour. Most of remaining tests will be devoted to conducting repeated spike overload/underload tests, but some will be used for testing under the standard TWIST [16] transport aircraft wing spectrum loading. These tests will be used to evaluate the current constraint-loss regime parameters, and develop a test method to evaluate proper regimes on both materials. All test specimens will be used to study the fracture behaviour for deep cracks ($c_i/w > 0.6$).

Ten Middle tension specimens manufactured from 7075-T7351 material are also available from DST Group. The specimens are 300 mm wide and 6.8 mm thick, and are from the same batch of testing which revealed issues under spectrum loading previously. Those specimens will be tested at the DST Group laboratory at Fishermans Bend Victoria, under the direction and input from Kevin Walker and another QinetiQ SI staff engineer.

5.1 Constant-Amplitude Loading, Constraint-Loss Behaviour and Fracture

Table 1 shows the test matrix for constant-amplitude loading. These tests were conducted to study the constraint-loss regime at several stress ratios. The new test data will be compared to the previous test data generated at NASA Langley Research Centre (LaRC) on the same material [8-13] and other relevant literature data. Fracture tests with anti-buckling guide plates will be conducted on all specimens to help validate the Two-Parameter Fracture Criterion (TPFC).

Table 1 – Test Matrix for Constant-Amplitude Loading.

Material	Constant-Amplitude Loading, R	Number of Specimens
2024-T3	0	2
	0.5	1
	0.7	1
7075-T6	0	3
	0.5	1
	0.7	3
7075-T7351	0	2
	0.5	2

5.2 Single-Spike Overload/Underload and TWIST Spectrum Testing

Table 2 shows the test matrix for the repeated single-spike overload and underload sequences. Three constant-amplitude cases will be considered, R = 0, 0.5 and 0.7. Various overload ratios, OL = P_{OL}/P_{max}, from 1.8 and 2.2 will be tested with several values of underload ratios, UL = P_{UL}/P_{max}, from 0.7 to -1.0 depending upon the R value. Only one specimen will be used for each test condition (see Figs. 6 and 11 for example).

Table 3 shows the test matrix for the TWIST spectrum loading tests. Level I is the full spectrum, while Level III is a truncated spectrum without the severe loading conditions.

FASTRAN will be used to pre-calculate each test, so that if a particular test shows some issues, a re-test using another specimen may be required.

Table 2 – Test Matrix for Repeated Spike-Overload/Underload Sequences.

Material	Constant-Amplitude Loading, R	S_{max}, MPa	OL = P_{OL}/P_{max}	UL = P_{UL}/P_{max}
2024-T3	0	55	1.8	0
		55	1.8	-1
		55	2.0	0
		55	2.0	-1
		55	2.2	0
		55	2.2	-1
	0.5	TBD	2.0	0.5
		TBD	2.0	0
	0.7	TBD	2.0	0.7
		TBD	2.0	0
7075-T6	0	75	2.0	0
		75	2.0	-1
		75	2.2	0
		75	2.2	-1
	0.5	TBD	2.0	0.5
		TBD	2.0	0
	0.7	TBD	2.0	0.7
		TBD	2.0	0

7075-T7351	0	75	2.0	0
	0.5	TBD	2.0	0
	0.7	TBD	2.0	0

Table 3 – Test Matrix for TWIST Spectrum Loading.

Material	TWIST Level	S_{max}, MPa	Number of Specimens
2024-T3	I	TBD	2
	III	TBD	1
7075-T6	I	TBD	2
	III	TBD	1
7075-T7351	I	TBD	2
	III	TBD	1

6. Statement of Work

(1) Conduct fatigue-crack-growth-rate tests on middle-crack-tension, M(T), specimens made of thin-sheet 2024-T3 and 7075-T6 aluminium alloy under constant-amplitude loading, repeated single-spike overload and underload sequences, and a special aircraft spectrum loading.

(2) Compare the ΔK-rate results from the M(T) specimens with previous test data generated at the NASA Langley Research Centre on the same materials, and other literature data as appropriate.

(3) Conduct fatigue-crack-growth analyses using the FASTRAN life-prediction code to study the constraint-loss behaviour under constant-amplitude loading, repeated single-spike overload and underload sequences, and the aircraft spectrum loading.

(4) Complete a final report on the test data and crack-growth analyses; and submit a paper to a journal.

(5) The testing at Mississippi State University can be completed by the end of calendar year 2022. The final reporting and project completion is estimated to be completed by 30 April 2023.

7. References

[1] Fatigue Crack Propagation, ASTM STP 415, American Society for Testing Materials, Philadelphia, PA, 1967.

[2] Schijve, J. “Significance of Fatigue Cracks in Micro-Range and Macro-Range”. Fatigue Crack Propagation, ASTM STP 415, 1967, pp. 415-459.

[3] Newman, J. C., Jr., “Discussion on Cyclic Crack Growth Transitional Behavior”. Fatigue Crack Propagation, ASTM STP 415, 1967, pp. 380-383.

[4] Elber, W. “The Significance of Fatigue Crack Closure”. ASTM STP 486, 1971, pp. 230-242.

[5] Newman, J. C., Jr., “FASTRAN II - Fatigue Crack Growth Structural Analysis Program, NASA TM-104159, February 1992.

[6] Newman, J. C., Jr., “FASTRAN—A fatigue crack growth life prediction code based on the crack-closure concept”, Version 5.4 User Guide, Fatigue and Fracture Associates, LLC, Eupora, MS, 2013.

[7] Donald, J. K. and Blair, A. “Automated Fatigue Crack Growth Testing and Analysis – Series 2001. Version 3.09, Fracture Technology Associates, LLC, Bethlehem, PA, 2009.

[8] Hudson, C. M. and Scardina, J. T. “Effect of Stress Ratio on Fatigue-Crack Growth in 7075-T6 Aluminum Alloy Sheet”. *Engineering Fracture Mechanics*, 1969, Vol. 1, pp. 429-446.

[9] Hudson, C. M. “Effect of Stress Ratio on Fatigue Crack Growth in 7075-T6 and 2024-T3 Aluminum Alloy Specimens”. NASA TN D-5390, 1969.

[10] Dubensky, R. G. “Fatigue Crack Propagation in 2024-T3 and 7075-T6 Aluminum Alloys at High Stress”. NASA CR-1732, 1971.

[11] Newman, J. C., Jr.; Wu, X. R.; Venneri, S. L. and Li, C. G., “Small-Crack Effects in High-Strength Aluminum Alloys - A NASA/CAE Cooperative Program, NASA RP-1309, May 1994.

[12] Newman, J. C., Jr. Fracture Analysis of Surface- and Through-Cracked Sheets and Plates. *Engineering Fracture Mechanics*, 1973, Vol. 5, pp. 667-689.

[13] Phillips, E. P. “The Influence of Crack Closure on Fatigue Crack Growth Thresholds in 2024-T3 Aluminum Alloys”. ASTM STP 982, 1988, pp. 505-515.

[14] Standard Test Method for Measurement of Fatigue Crack Growth Rates, ASTM E-647, 2016.

[15] Newman, J. C., Jr., “Fracture Analysis of Various Cracked Configurations in Sheet and Plate Materials,” Properties Related to Fracture Toughness. ASTM STP 605, 1976, pp. 104-123.

[16] de Jonge, J. Ii., Schutz, U., Lowak, H. and Schijve, J., A Standardized Load Sequence for Flight Simulation Tests on Transport Aircraft Wing Structures, LBF-Bericht FB-106, NLR TR 73029 U, March 1973.

8.0 Budget

Item	$USD thousands	Completion Date
1. Testing of 2024-T3 and 7075-T6 specimens at Mississippi State University as per this document		31 December 2022
2. Development of updated model for constraint loss, spike overloads, spectrum loading and fracture. Contribute to Technical Report and Journal paper		30 April 2023
Total		

Notes:

1. Items 1 and 2 will be performed at the Mississippi State University Aerospace Engineering Department mechanical test laboratory, under the direction of Professor Jim Newman, and in collaboration with Dr Kevin Walker from QinetiQ Australia. Payment to be directed through Fatigue Technology Associates (FTA).